Journal of Applied Polymer Science

Structure-property relationships in copolyester elastomer-layered silicate nanocomposites

Eid M. Alosime, Grant A. Edwards, Darren J. Martin
Australian Institute for Bioengineering and Nanotechnology, The University of Queensland, QLD 4072, Australia
Correspondence to: D. J. Martin (E-mail: darren.martin@uq.edu.au)

ABSTRACT: While the field of polymer–clay nanocomposites is reaching maturity, some parts of the studied systems still present researchers with possibilities for the improvement of material properties. This study entails the understanding of the relationships in copolyester elastomer/organically modified layered silicate nanocomposite and the structure–property relationships within the system of the nanocomposite. A series of these nanocomposites was prepared via twin-screw extrusion melt compounding. The experiments included the following three types of synthetic organosilicates: high aspect ratio Somasif (ME100) fluoromica and two lower aspect ratio Laponite synthetic hectorites, (WXFN) and (WXFP). These organosilicates were modified with quaternary octadecyltrimethylammonium bromide (ODTMA) and were used to prepare the nanocomposites. The nanocomposite structure on a micro- and nanometre scales was evaluated by two techniques, such as X-ray diffraction (XRD) and transmission electron microscopy (TEM). The mechanical properties of the nanocomposites were examined to determine the impact aspect ratio of the nanofiller and wt % loading have on performance. The addition of the 2 wt % high aspect ratio of ME100-ODTMA, in particular, showed statistically improved tensile strength, tear resistance, creep resistance, and water vapor permeation barrier enhancement. © 2014 Wiley Periodicals, Inc. J. Appl. Polym. Sci. **2015**, *132*, 41742.

KEYWORDS: creep resistance; organoclay; thermoplastic polyester elastomer; water vapour permeability

Received 29 August 2014; accepted 6 November 2014
DOI: 10.1002/app.41742

INTRODUCTION

In the nanotechnology sector, the research and development of polymer nanocomposite materials has gained significant scientific and commercial interest, with a gamut of new nanocomposite systems now extending the application areas of traditional polymeric materials. These application extensions can be attributed to the recent enhancements of a range of properties, such as high-temperature resistance and dimensional stability, barrier properties, and other mechanical properties, including strength, toughness, abrasion, and creep resistance.[1,2]

Thermoplastic polyester elastomers (TPE-E) are high-performance thermoplastic alternatives to natural or synthetic cross-linked rubbers. TPE-E materials are segmented block copolymers typically incorporating hard (polyester) blocks and soft (polyether) blocks. These materials have compositions, structures, and morphologies that make them highly useful. Industrially, TPE-E materials are valued for their thermoplastic qualities, stable structures, and easy thermal processability. Hytrel® is a trademarked brand of DuPont for TPE-E (copolyesters, COPEs) thermoplastic elastomers. It is marketed as a thermoplastic that "provides the flexibility of rubber, the strength of plastics, and the processability of thermoplastics."[3] According to the product description, Hytrel is a polyether–ester block copolymer with several available grades that can be specialized for flexibility, resistance to impact, extreme temperature, and fatigue tolerances. Hytrel is also unaffected by industrial chemicals, oils, and solvents, though protection from UV exposure is advised. The mechanical strength and durability of Hytrel allows it to be used for a variety of applications, including seals, bushings, and belts. Other applications include pump diaphragms and gears used in the automotive industry, which require exceptional fatigue resistance.[3] Furthermore, its low permeability to refrigerant gases and nonpolar hydrocarbons makes it an effective conduit for transmitting gas for heating, cooking, and refrigeration.[3] Hytrel polymers have a high degree of permeability to polar substances such as water, which limits their applicability in areas where water impermeability or hydrothermal stability are required.[4] The incorporation of nanofillers is observed as one promising strategy to address this limitation.

Because of the increasing demand for environmentally friendly products, DuPont has also produced a variant of Hytrel, called Hytrel® RS Renewably Sourced, which is comprised of 35–65% renewably sourced materials without compromising quality.[3] Because of the seemingly limitless ways that TPE-E materials can be modified for different uses, many manufacturers other

than DuPont have been experimenting with thermoplastic elastomers. For example, Walia *et al.*[5] polymerized a poly(hydroxy ester ether) (PHEE) material, which has pendant hydroxyl groups along the polyester backbone. According to the researchers, the hydrophobic PHEE had a reduced permeability to water vapor compared to Hytrel, which is water-permeable. However, the PHEE grade shows a high sensitivity to the water content in terms of its mechanical properties. Several studies have demonstrated the relationship between mechanical properties and moisture in PHEE. The modulus and tensile strength were observed to decrease with an increase in the moisture content. For instance, PHEE's modulus can decrease from a value of 1000 MPa at 0% RH to about 40 MPa at 50% RH.[6] This is caused by a shift in the T_g of PHEE from 45°C in its dry state to 10°C at 5% moisture.[7]

Some research has been performed in the field of TPE-E, and experimentations have yielded new copolymers with better properties. For instance, Versteegen *et al.*[8] showed that segmented copoly(ether urea)s with two uniform hard blocks of two urea groups possess better mechanical properties than most commercially available TPE-E. Several structural modifications have also been attempted on Hytrel to yield polymers with better properties. Such experimentations have also been performed to gain an understanding of the properties and morphology of Hytrel. Studies by Aso *et al.*[9] have shown that the addition of fumed silica (SiO_2) to Hytrel resulted in an improved creep resistance. Sreekanth *et al.*[10] investigated how the addition of fly ash and mica affected the mechanical properties of Hytrel. They showed that the presence of these fillers in the polymer led to an increase in its modulus, flexural strength, and thermal and electrical properties. Morphological studies reveal that the fillers well throughout the polymer at low concentrations. In some studies, UV irradiation of Hytrel has led to dramatic morphological changes due to photo-oxidation.[11] This photo-oxidation leads to a mixed morphology by improving the compatibility of the two phases.

To achieve optimal nanocomposite formation, the four following structural variables must be considered: (1) an engineered low and high aspect ratio nanofiller, (2) nanofiller uniform distribution and dispersion, (3) alignment of the nanofiller in the polymeric matrix, and (4) polymer–nanofiller interfacial stress transfer.[12–16] The resultant molecular interaction between the polymer matrix and the (potentially) large organoclay surface area (760 m^2/g)[17] increases stress transfer to the reinforcement phase, which enables toughening and tensile strength enhancement. In addition, layered silicate thicknesses are approximately 1 nm, and aspect ratios can range from 10–1000 for organoclay particulates.[18]

There are various explanations for the increased gas barrier performance in polymer nanocomposites. According to Yano *et al.*,[19] it is possible to enhance the barrier resistance by incorporating the high aspect clay into the host matrix, which makes it difficult for the penetrant to travel by increasing the tortuosity of the pathway. Alternatively, the presence of the nanofillers within the host matrix may change its diffusivity by reducing the free volume of the matrix or simply changing its orientation.[20–22]

Although the strong interfacing of discrete, high aspect ratio nanofillers is ideal for the most efficient reinforcement of any host polymer, this is difficult to achieve in practice. This difficulty can be attributed to the inherent face-to-face stacking present in agglomerated organoclay tactoids, combined with the differences in compatibility between the hydrophilic-layered silicates and hydrophobic plastics.[17] Among the types of layered silicate nanofillers, synthetic fluoromica, and fluorohectorite-layered silicates are among the most important classes of nanofillers. For this study, three different synthetic silicates were selected as nanofillers due to their different sizes and aspect ratios, to investigate the influence of nanofiller morphology on mechanical and barrier properties.

Alkylammonium surfactants are usually used to modify clays for better interactions between the hydrophilic aluminosilicate and the organophilic polymer matrix, and to best facilitate an exfoliated nanocomposite structure.

The study of TPE-layered silicate nanocomposites is still relatively immature. Previously, Hytrel nanocomposites were synthesized through a melt-compounding process for improvements in viscoelastic properties.[23] So far, there have been no investigations in the literature of Hytrel 3078 nanocomposites being prepared via twin-screw extrusion, and there have been no thorough studies into the effects of low and high aspect ratio silicate clays on the microstructure. In this study, we first modified the clay surfaces to make them more compatible with a Hytrel matrix. TPE-E nanocomposites were prepared by twin-screw extrusion using modified and unmodified silicates. The effects of well-dispersed organophilic clays on the structure and properties were also investigated.

EXPERIMENTAL

Materials

The thermoplastic polyester elastomer Hytrel 3078 grade with nominal hardness of 30D was purchased from DuPont™.[3] Somasif ME100 with a cation-exchange capacity (CEC) of 110 mequiv/100 g and an aspect ratio of 500–1000 nm/1 nm was purchased from Kobo Products, Inc. (New Jersey).[24] Laponite WXFN and WXFP with a cation-exchange capacities (CEC) of 120 mequiv/100 g, and aspect ratios of 120 and 80 nm/1nm, respectively, were purchased from Rockwood Additives Ltd. (UK). Octadecyltrimethylammonium bromide (ODTMA) was purchased from Sigma-Aldrich (Castle Hill, Australia). The water was purified using a Milli-Q Academic system (Merck Millipore, Merck Ltd., Kilsyth, Australia) (conductivity 18.2 μS and pH 6.8).

Nanofiller Surface Modification

The clay modification was carried out by replacing its sodium ion with quaternary alkylammonium groups from ODTMA through an ion-exchange process in an aqueous solution. Approximately, 1 wt % of clay was dispersed in water at 60°C for 24 h with continuous stirring. The organoclays were washed with water, centrifugated and separated from the supernatant several times to remove the unbound surfactants and salts (NaCl and NaBr). This process was stopped when no precipitation was detected in the supernatant after the addition of 0.1*M* $AgNO_3$. The modified clay was dried in a vacuum oven overnight at 60°C and subsequently grinded and then milled using a

Table I. The Temperature Profile and Other Parameters Used in the Extrusion Process

T1	230°C
T2	240°C
T3	255°C
T4	240°C
T5	235°C
T6	220°C
T7	220°C
T8	215°C
T9	205°C
T10	190°C
Diameter of the die	3 mm
Screw speed	90 rpm
Torque	60%

Micron Master® Jet Pulverizer (The Jet Pulverizer Co., New Jersey). ME100-ODTMA refers to Somasif ME100, which was modified with 100% ODTMA (i.e., equivalent moles of surfactant with respect to supplier's CEC values). WXFN-ODTMA and WXFP-ODTMA refer to Laponite WXFN and WXFP, which were also modified with 100% ODTMA.

Nanocomposite Preparation

Initially, Hytrel nanocomposites with three different types of organically modified clays and a series of clay loadings of 1–4 wt % were prepared for mechanical testing. An appropriate Hytrel control was prepared with the identical thermal processing history. Before processing, Hytrel and the raw silicate/organosilicate series of ME100, ME100-ODTMA, WXFN, WXFN-ODTMA, and WXFP, WXFP-ODTMA were dried in a vacuum oven at 80°C and 60°C for 3 and 24 h, respectively. Hytrel and clays/organoclays were melted and compounded in a Thermo Haake® PolyLab Twin-Screw Extruder (corotating, 16 mm screw dia. with a L/D of 40). The extrusion parameters used in the melt processing are displayed in Table I. The extrudate from the die was pelletized and dried in a vacuum oven at 80°C for 3 h prior to compression molding at 190°C. Approximately, 1 mm thick plaques were pressed and annealed in a vacuum oven at 80°C for 12 h and left to age for 1 week prior to testing.

X-ray Diffraction (XRD) Study

XRD was performed at room temperature using a Bruker D8 Advance X-ray diffractometer. The X-ray beam was nickel filtered Cu K_α radiation operated at 40 kV and 30 mA. Data were recorded in the range of $2\theta = 1°–10°$ using an increment of 0.02° and scan rate of 2.4°/min.

Transmission Electron Microscopy (TEM)

TEM photograph of thin layer of the samples was recorded using a JEOL 1011 TEM operated at 100 KeV. The thin layer of samples was prepared using a Leica Ultracut UC6FCS microtome (Leica Microsystems Pty Ltd., North Ryde, Australia), equipped with cryosectioniong unit. The samples were sliced into thin layers of about 90 nm by a diamond knife cooled at −110°C.

Dynamic Mechanical Thermal Analysis (DMTA)

DMTA measurement was carried out using a Mettler Toledo dynamic mechanical analyzer 1 Star and the device operated under a tensile head and reducing force option. The test was subjected to a frequency of 2 Hz and a heating rate of 2°C/min in tension mode.

Differential Scanning Calorimetry (DSC)

DSC analysis was carried out using the Mettler Toledo differential scanning calorimeter 1 Star. About 6–9 mg of sample was heated from −100°C to 280°C at heating rate of 10°C and then cooled to 25°C at the same ramping rate.

Mechanical Testing

Mechanical properties measurement was taken at room temperature using an Instron Model 5543 universal testing machine with a capacity of 500-N load cell. The average of 5 and 3 replicates of each sample for tensile and tear tests, respectively, is reported here. The samples were cut into a dumbbell shape from an ASTM D-638-M-3 die, and a crosshead speed of 50 mm/min was applied for tensile test, while the creep test was conducted according to ISO 899-1:2003, with a stress of 3.5 MPa and a 6-h holding time.

Water Vapor Permeation

Through the sample, the water vapor permeability of the films was studied using a PERMATRAN-W 3/31 instrument (MOCON, Minneapolis, MN) operated at 23°C, 1 atm and 100% RH. The water vapor transmission rate was normalized with respect to film thickness.

RESULTS AND DISCUSSION

Nanocomposite Structure

Nanocomposite structure was characterized using XRD and TEM. XRD defined the shape intensity and amount of basal reflection from the organosilicate platelet layers. When the polymer chains were intercalated between the layered silicates, there was an increase in silicate interlayer distance, which gave rise to a shift of the 001-diffraction peaks to lower angles. In the exfoliated structures where silicate layers were reasonably distributed in a continuous polymer matrix, no diffraction peaks were observed. A broadening of this diffraction pattern can indicate partial exfoliation of the silicate layers as crystallite size and degree of registration is decreased. Figure 1a shows the XRD patterns for pristine ME100, ME100-ODTMA, and the corresponding patterns of Hy3078/ME100-ODTMA nanocomposites with various amounts of ME100-ODTMA in the diffraction angle range $2\theta = 2–10°$. Diffraction ranging from $2\theta = 2–10°$ indicated an intercalated hybrid or an immiscible system. The 001 diffraction peak indicated for ME100 appeared at $2\theta = 7–10°$, of which the interlayer distance was 1.24 nm. The presence of alkyl ammonium ions in the basal spacing reduced the attractive forces between the clay and enabled the polymer to be intercalated into the clay galleries, thereby aiding the dispersion of the clay. The smaller interlayer distance at higher clay content was attributed to the increased number of intercalated structures with increased pristine clay or organoclay content, which

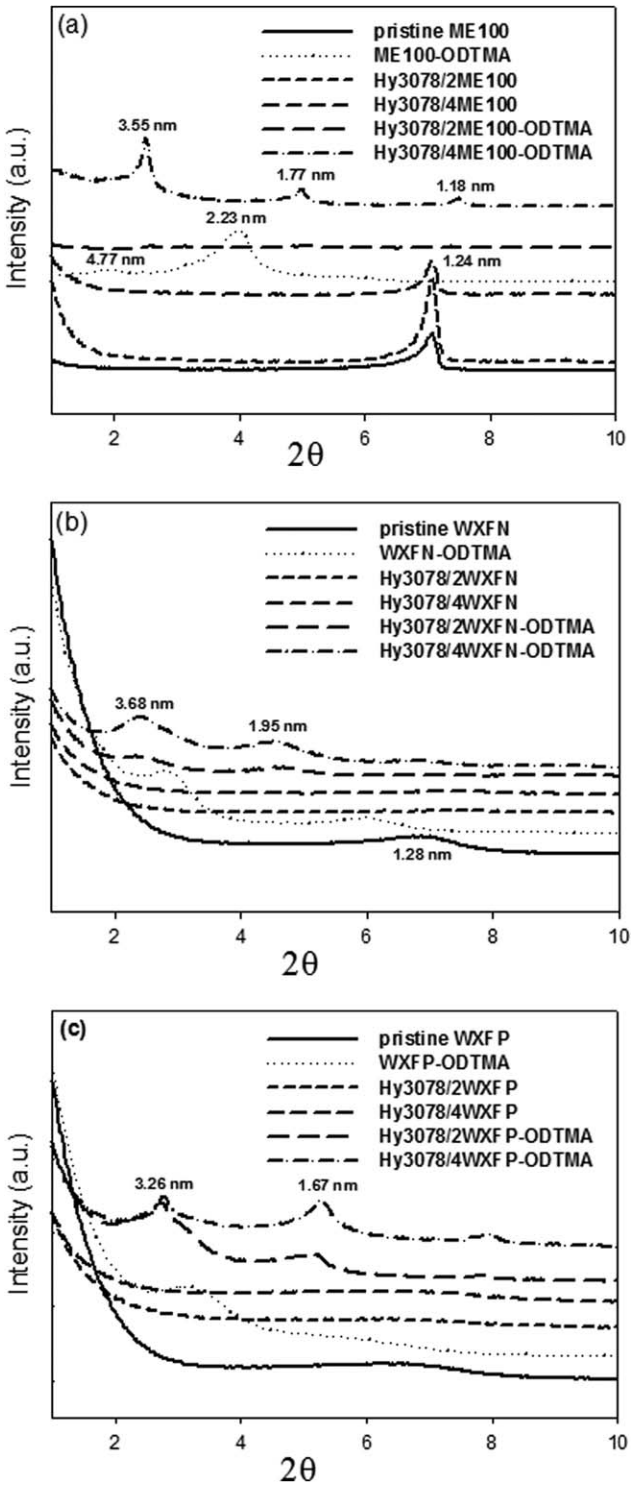

Figure 1. XRD patterns of the (a) pristine ME100, ME 100-ODTMA, and Hy3078 composite and nanocomposites (b) pristine WXFN, WXFN-ODTMA, and Hy3078 composites and nanocomposites (c) pristine WXFP, WXFP-ODTMA, and Hy3078 composites and nanocomposites.

might have impeded the higher basal spacing or exfoliation of individual silicate layers.[25] Figure 1b represents XRD patterns for pristine WXFN, WXFN-ODTMA, and the corresponding patterns of Hy3078/WXFN-ODTMA nanocomposites. The interlayer gallery height for the pristine WXFN, the distance of $d(001)$ and the individual layer thickness (≈1 nm), was 1.28 nm (2θ=6.90°). The XRD profile of Hy3078 composites showed a nearly exfoliated structure of the dispersed silicate layers in Hy3078/WXFN matrix, but in the case of Hy3078/WXFN-ODTMA with 4 wt % clay content, it indicated a disordered intercalated structure with a (001) plane peak at 2θ=2.40° (=3.68 nm). In Figure 1c, the XRD profile of the pristine WXFP and their respective composites showed the same trend as that of WXFN. This suggests that as the filler content increases, the mobility of the nanofiller is decreased, providing low-driving force for the intercalated polymer to break the tactoids. However, 2ME100-ODTMA showed orderly diffraction peaks in comparison to the pristine ME100, associated with interlayer distances 4.7, 2.2, and 1.6 nm, respectively. Extra peaks were as a result of longer range registration and interstratified superstructure of the largest ME100 synthetic clay, which originates from a well-published inherent charge heterogeneity.[26,27] This charge heterogeneity might have allowed different amounts of surfactant chains to intercalate the fluoromica layers; therefore, monolayer–bilayer or bilayer pseudotriple-layer arrangements were possible.[26,27] The high aspect ratio ME100 could result in long-range order of organosilicate tactoids that would have contributed to the strong diffraction peaks in the resulting organosilicate tactoids (with respect to synthetic WXFN and WXFP or natural nanosilicates).

TEM micrographs are arguably the most direct way to observe the intercalated or exfoliated structure of the organoclay nanofillers in the nanocomposites compared to the pristine clays. All TEM images are of Hy3078-based nanocomposites with 2 wt % at low (27,500×) and high (60,000×) magnification. Figures 2(a, c, and e) show typical TEM images for Hy3078/2ME100, Hy3078/2WXFN, and Hy3078/2WXFP. It was apparent that unmodified ME100, WXFN, and WXFP existed as a large synthetic clay agglomerates in the Hy3078 matrix. This was due to the incompatible nature of these high surface energy constituents. As shown in the XRD result, there was no shifting in the diffraction peak of the pristine clay Hy3078 composites. However, all the organoclays (ME100-ODTMA, WXFN, and WXFP; Figures 2b, d, and f) were intercalated or exfoliated into nanosized particles or aggregates. The silicate layers were dispersed homogeneously as observed in the cryosections of all of the nanocomposites. These results matched with the XRD results that indicated that these nanocomposites produced intercalated and exfoliated structure types. In conclusion, we can deduce that high aspect ratio of ME100, which has lower mobility and higher space restrictions experiences frustrated orientational freedom in the matrix, making it hard for the intercalated Hy3078 to fleece platelets from the well-structured tactoids.[28]

Mechanical Properties

The effects of pristine clay and organoclay loading on the mechanical properties of melt compounded Hy3078 (pure Hy3078 and composites) are summarized in Table II. Achievement of ideal mechanical properties was when 2 wt % ME100-ODTMA was incorporated, increasing the tensile and tear strength by 17% and 10%, respectively. Up to 2 wt % filter loading, the organoclays are uniformly dispersed and gives rise

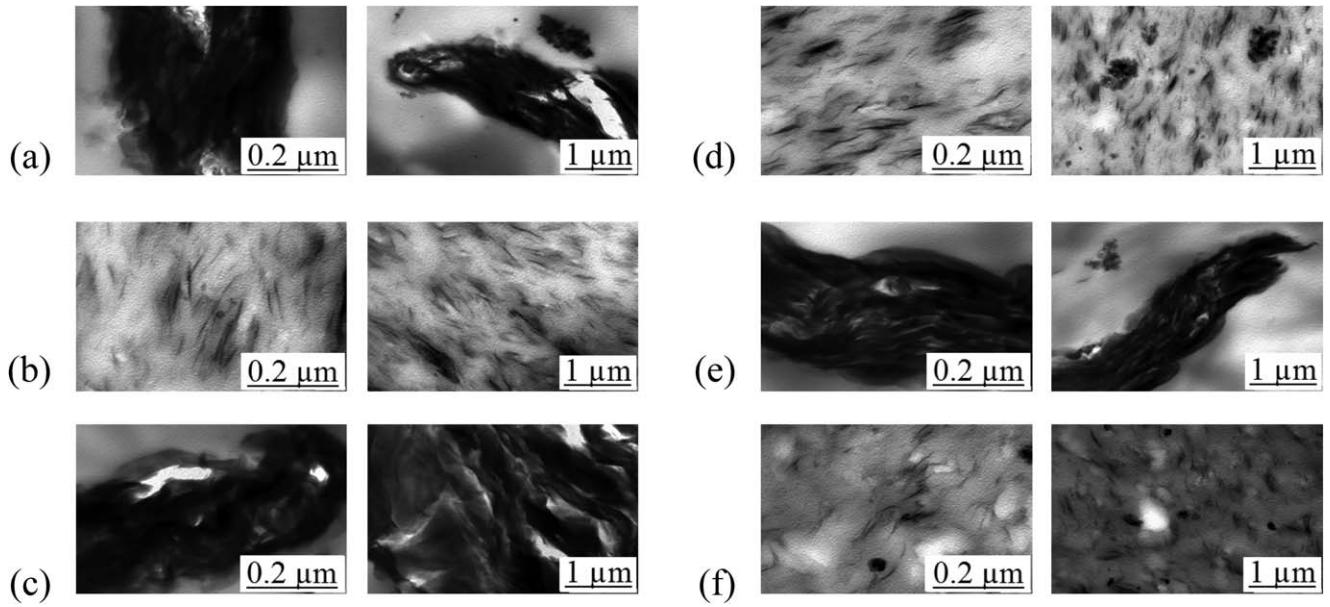

Figure 2. TEM images of Hy3078/2ME100 (a), Hy3078/2ME100-ODTMA (b), Hy3078/2WXFN (c), Hy3078/2WXFN-ODTMA (d), Hy3078/2WXFP (e), and Hy3078/2WXFP-ODTMA (f) at low (27,500×) and high (60,000×) magnification.

to well-intercalated or exfoliate morphologies in the Hy3078 matrix, as has been reported in the TEM results. The organoclay platelets of ME100-ODTMA possessed a very high aspect ratio were more efficient reinforcing elements, assuming reasonable filler-polymer interactions.[29] The tensile strengths of WXFN and WXFP decreased with the incorporation of filler. The slightly higher degree of nanofiller agglomeration in these systems, combined with a platelet size which could be considered below the critical diameter required for effective reinforcement, reduced tensile strength.[30] Reagglomeration at higher organoclay content is because the amount of matrix molecules becomes fewer than those required for a complete exfoliation (this means molecules of the polymer and those of intercalating compounds of organoclay intermingle). In practice, the much longer extruder residence time that would be required for supreme dispersion at higher nanofiller loadings would be associated with other deleterious problems such as thermal degradation and loss of TPE molecular weight, so these processability contraints are also important to consider. For elongation properties, the elongation at break for pure Hy3078 was 2075%, which decreased alongside other composites and nanocomposites to various extents after the incorporation of fillers into the polymer matrix. This indicated an interruption of the mobility or deformation of the matrix through the physical interaction and immobilization of the polymer matrix in the presence of mechanical restrains.[10] Table III shows that Young's modulus for the composites and nanocomposites increased continuously with increasing clay content, especially Hy3078/ME100-ODTMA, which achieved almost 16 MPa, up from approximately 9 MPa for the host. The improvement of the modulus has been attributed to the good dispersion of nanosized clay particles that hinder the mobility of polymer chains under loading and good interfacial adhesion of the clay interlayer and the polymer as reported by several researchers.[9,31] The tensile creep analysis was performed for a few samples to determine their time-dependent dimensional stability under tensile deformation. The tensile creep modulus (E_t) (ratio of the stress applied to the strain of tensile creep) was used to determine the creep resistance of the Hy3078 and the Hy3078/ME100 composites and nanocomposites. E_t values for pure Hy3078, Hy3078/ME100, and Hy3078/ME100-ODTMA measured at 3.5 MPa creep resistance are shown in Table III and their representative tensile creep curves in Figure 3. The highest E_t was achieved by Hy3078/2ME100-ODTMA, with an increase in 18%. This proved that the highest aspect ratio and best dispersed organoclay was at a position to raise creep resistance and stability of the Hy3078.

Differential Scanning Calorimetry

The DSC cooling and subsequent heating scans of the pure Hy3078, Hy3078/ME100, Hy3078/WXFN, and Hy3078/WXFP composites and nanocomposites are shown in Figures 4(a, c, and e) and Figures 4(b, d, and f), respectively, while the summary of DSC features is as shown in Table IV. Addition of the fillers increased the crystallization temperature (T_c) up to 16°C. Even at amounts as high as 4 wt %, a notable increase in the T_c of Hy3078/ME100 was observed, while the T_c increased by approximately 10°C with both Hy3078/WXFN and WXFP compared to the pure Hy3078. This indicates that the clay played a role in reducing the chain mobility and promoting the crystallization as a nucleation agent.[23] In a previous DSC analysis by Aso *et al.*[9] on nanosilica-based Hytrel nanocomposites, it was shown that the T_c while it was being cooled increased from 155°C in the pure Hytrel to 163°C in the nanocomposites, but the crystalline content of PET increased with fumed silica content, both modified and unmodified.[32] and epoxy-modified fumed silica nucleated the crystallization of a propylene-ethylene copolymer.[33] From the heating scan, we observed three

Table II. Summary of Tensile Properties

	Filler (wt %)		Tensile strength (MPa)	Young's modulus (MPa)	Elongation at break (%)	Tear strength (MPa)
Hy3078	-		34.4 ± 0.8	8.8 ± 1.1	2157 ± 63	91.6 ± 4.9
	1	ME100	30.6 ± 1.3	12.0 ± 1.4	1830 ± 59	82.4 ± 1.7
		ME100-ODTMA	38.1 ± 0.9	13.1 ± 1.0	2054 ± 50	93.8 ± 3.6
		WXFN	25.3 ± 0.6	9.1 ± 0.1	1674 ± 34	75.2 ± 1.8
		WXFN-ODTMA	24.5 ± 1.1	9.2 ± 0.8	1643 ± 33	89.1 ± 1.6
		WXFP	24.9 ± 0.9	8.4 ± 0.6	1720 ± 26	86.6 ± 1.9
		WXFP-ODTMA	27.4 ± 0.5	8.8 ± 0.2	1750 ± 27	83.5 ± 2.0
	2	ME100	31.3 ± 0.8	10.1 ± 0.7	1824 ± 54	86.8 ± 1.1
		ME100-ODTMA	41.5 ± 3.4	16.0 ± 0.9	2033 ± 74	101.7 ± 13.3
		WXFN	28.6 ± 0.6	8.9 ± 0.5	1748 ± 53	64.5 ± 2.6
		WXFN-ODTMA	27.4 ± 1.2	9.2 ± 1.7	1765 ± 57	49.1 ± 1.7
		WXFP	22.5 ± 0.6	9.0 ± 0.7	1704 ± 30	86.1 ± 1.0
		WXFP-ODTMA	26.2 ± 1.0	12.6 ± 0.8	2039 ± 32	53.9 ± 2.9
	3	ME100	34.6 ± 1.2	10.7 ± 1.3	1988 ± 63	92.0 ± 5.4
		ME100-ODTMA	37.7 ± 1.9	12.9 ± 0.6	2002 ± 69	93.3 ± 5.0
		WXFN	26.7 ± 1.9	9.1 ± 0.7	1674 ± 34	55.3 ± 1.5
		WXFN-ODTMA	26.0 ± 0.6	8.5 ± 0.3	1673 ± 41	55.7 ± 0.7
		WXFP	22.9 ± 0.6	8.0 ± 0.7	1501 ± 57	80.6 ± 2.2
		WXFP-ODTMA	25.1 ± 0.9	8.2 ± 0.9	1636 ± 56	47.8 ± 2.2
	4	ME100	35.0 ± 0.7	10.1 ± 0.5	2036 ± 24	98.1 ± 2.0
		ME100-ODTMA	36.4 ± 1.3	13.6 ± 0.2	1872 ± 73	92.5 ± 3.8
		WXFN	26.3 ± 0.5	9.4 ± 0.7	1689 ± 37	56.8 ± 0.4
		WXFN-ODTMA	23.3 ± 0.6	9.5 ± 0.3	1561 ± 57	80.6 ± 2.2
		WXFP	19.7 ± 0.3	7.4 ± 0.3	1365 ± 28	77.2 ± 1.8
		WXFP-ODTMA	25.0 ± 0.9	8.4 ± 0.7	1643 ± 54	46.7 ± 0.9

to four endotherms, and they have been labeled T1–T4. A discrete soft segment glass transition at approximately −70°C was found in all samples. Addition of filler did not affect the temperatures or the enthalpy associated with the endotherms. The T1 endotherm was observed at 5°C in all samples. This endotherm may have been attributed to distortion of the hard segment consisting molecular units of esters. Immediately, a broad exotherm was seen after the T1 endotherms, and it is believed to be in relation to conformational changes in the hard phase following the melting of endotherms. The samples with WXFN showed a disappearance or a weak endotherm of T2 at temperatures between 48–58°C which was not resolved in Figure 3d. This weak endotherm that disappears after annealing below the melting temperature is probably caused by the melting of crystalline aggregates of soft segments formed in these copolyester composites not yet in equilibrium.[34]

Table III. Tensile Creep Modulus (E_t) of the Hy3078 and Hy3078/ME100-ODTMA Nanocomposites

	Filler (wt %)	Tensile creep modulus (MPa)
Hy3078	-	13.9 ± 0.6
	2ME100	11.2 ± 1.1
	2ME100-ODTMA	17.2 ± 0.8
	4ME100	15.4 ± 0.5
	4ME100-ODTMA	11.2 ± 1.1

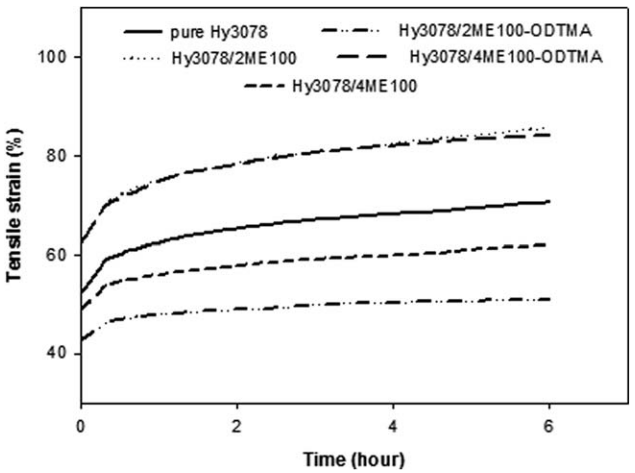

Figure 3. Tensile creep curves of Hy3078, Hy3078/2ME100, Hy3078/4ME100, Hy3078/2ME100-ODTMA, and Hy3078/4ME100-ODTMA at an applied stress of 3.5 MPa.

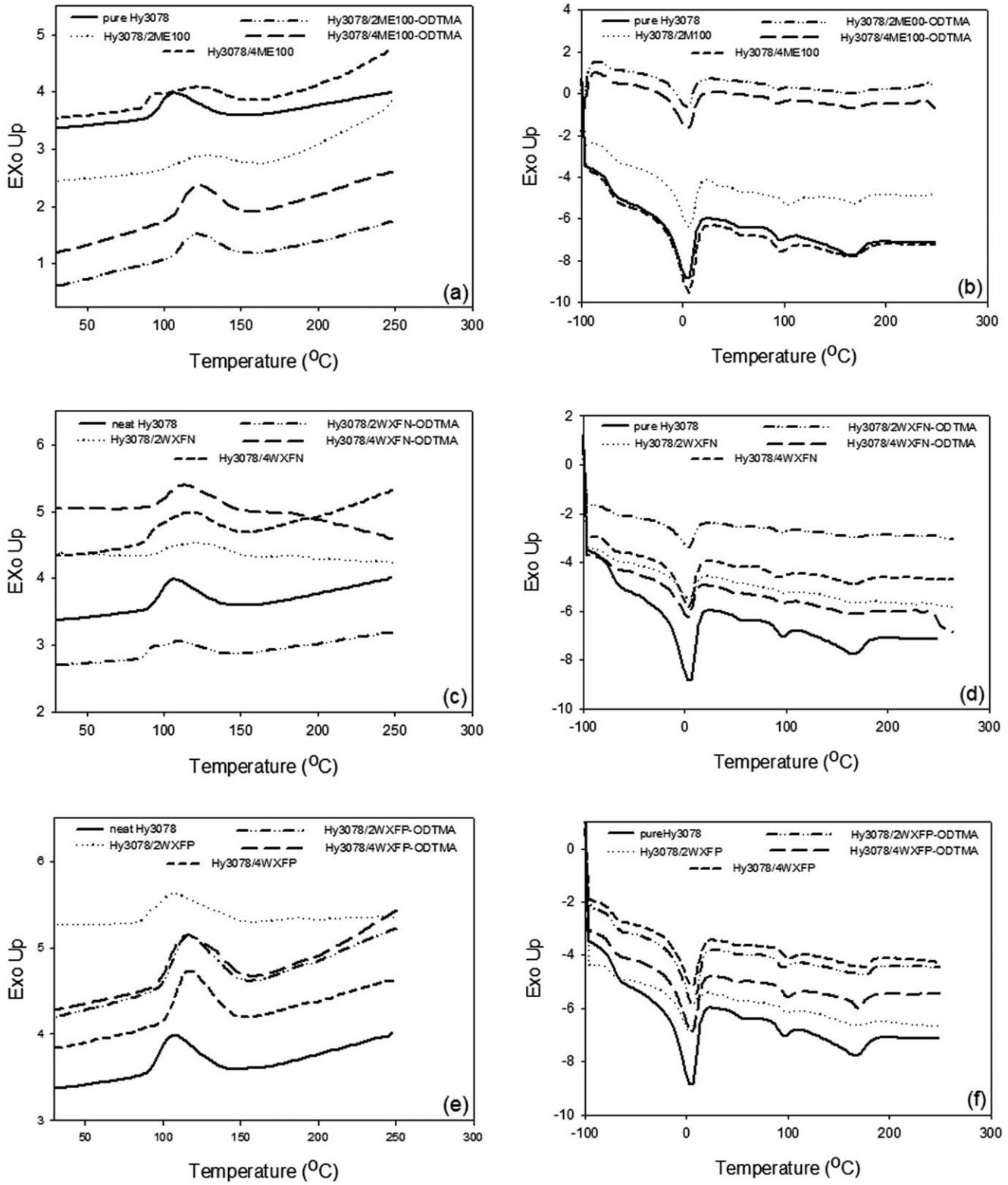

Figure 4. DSC thermograms of cooling and heating for different Hy3078 with various clays: a, b Hy3078/ME100 and nanocomposites; c, d Hy3078/WXFN and nanocomposites; e, f Hy3078/WXFP and nanocomposites, respectively.

Dynamic Mechanical Properties

The plots of the tan δ and storage modulus (E') versus temperature for pure Hy3078 and their composites are shown in Figure 5. The tan δ peak values [Figures 5(a, c, and e)] for soft segment glass transition temperatures are given in Table V. The aspect ratio of the organoclay employed brings about subtle differences

Table IV. Summary of DSC Heating and Cooling Curves

			Heating							Cooling	
			Endotherm peaks					Exotherm		Crystallization exotherm	
Matrix	Nanofiller	T_g (soft)	T1 (°C)	T2 (°C)	T3 (°C)	T4 (°C)	Hard Phase ΔH_m (J/g)[a,b]	Peak (°C)	ΔH (J/g)[b]	Peak (°C)	ΔH_c (J/g)[b]
Hy3078	-	−70	4.4	56.8	95.0	165	33.9	-	-	106	8.4
	2ME100	−68	5.5	56.8	94.7	171	29.2	-	-	125	6.6
	4ME100	−69	5.8	57.8	96.0	164	31.9	-	-	119	8.6
	2ME100-ODTMA	−75	3.9	51.8	92.1	166	43.1	241	9.9	121	8.9
	4ME100-ODTMA	−76	4.3	49.5	92.1	168	35.1	234	5.2	122	10.2
	2WXFN	−68	3.7	-	96.3	166	31.8	-	-	122	8.0
	4WXFN	−69	3.5	-	90.0	166	33.1	-	-	115	9.4
	2WXFN-ODTMA	−70	2.8	-	91.7	161	40.0	242	7.6	112	9.2
	4WXFN-ODTMA	−68	2.5	-	94.9	165	32.6	-	-	113	10.2
	2WXFP	−68	3.5	51.1	97.6	164	32.85	-	-	107	8.9
	4WXFP	−75	5.0	49.2	100	162	29.5	-	-	116	9.0
	2WXFP-ODTMA	−71	6.2	50.2	94.5	177	30.8	-	-	116	9.3
	4WXFP-ODTMA	−72	5.0	48.5	99.1	169	31.2	-	-	114	9.6

[a] Enthalpy of fusion values is the sum of the T1–T4 melting enthalpies.
[b] Enthalpies were calculated per gram of hard segment (not per gram of sample).

in the DMTA responses, presumably due to variations in degree of nanofiller dispersion and intercalation, as well as relative phase and filler length scales and dynamic mobility of the fillers. Additional small shoulders seen at $T > T_g$ may be due to the existence of a hard-soft segment interphase layer with slower dynamics[9], and this signature appears more pronounced for the WXFN-reinforced composites suggesting more effective restraint of this interfacial zone by the intermediate aspect ratio nanofiller.[35] This phenomenon also appears to correlate with the suppression, or disappearance of the weak T2 DSC endotherm. When performance of WXFP composites is compared to Hy3078, the higher tan δ values of Hy3078 with modified WXFP-ODTMA indicate an elastic contribution of the filler. The different response was attributed to the presence of the quaternary ammonium modification despite the full elastic response of the inorganic filler at the levels of stress. This difference in response is due to an increase in the amount of the noncrystalline hard segments in the amorphous phase or an increase in the mobility of the soft phase.[36] The unusual decrease in the soft segment T_g peak temperature for unmodified WXFP composites compared with the pure Hy3078 is potentially due to some weak preferred nanofiller interaction with the hard segment population, thereby reducing hard-soft domain phase mixing, so that the T_g of the soft segment is decreased. The storage modulus of the Hy3078 and their composites are shown in Figures 5(b, d, and f). In particular, an increase in storage modulus was observed for Hy3078/4WXFP-ODTMA compared to Hy3078/2WXFP-ODTMA indicating that the presence of organoclays has much more significant effects on the elastic properties than on the viscous ones at a low concentration range.[23]

Table V. Transition Temperatures (T_g) Determined from DMTA Curves

Matrix	Nanofiller	Glass transition temperature, T_g (°C)
Hy3078	-	−50.2
	2ME100	−51.2
	4ME100	−49.6
	2ME100-ODTMA	−48.3
	4ME100-ODTMA	−49.6
	2WXFN	−51.6
	4WXFN	−50.4
	2WXFN-ODTMA	−51.2
	4WXFN-ODTMA	−50.0
	2WXFP	−58.7
	4WXFP	−59.1
	2WXFP-ODTMA	−50.8
	4WXFP-ODTMA	−51.2

Water Vapor Permeability Tests

Based on the previous results, only the selected nanocomposite systems that showed the best mechanical performance are discussed in the following permeability test results. Table VI summarizes the results of the water vapor permeability tests for pure Hy3078 and its nanocomposites Hy3078/2ME100-ODTMA and Hy3078/4ME100-ODTMA. The water vapor permeability decreased when ME100-ODTMA was incorporated into the

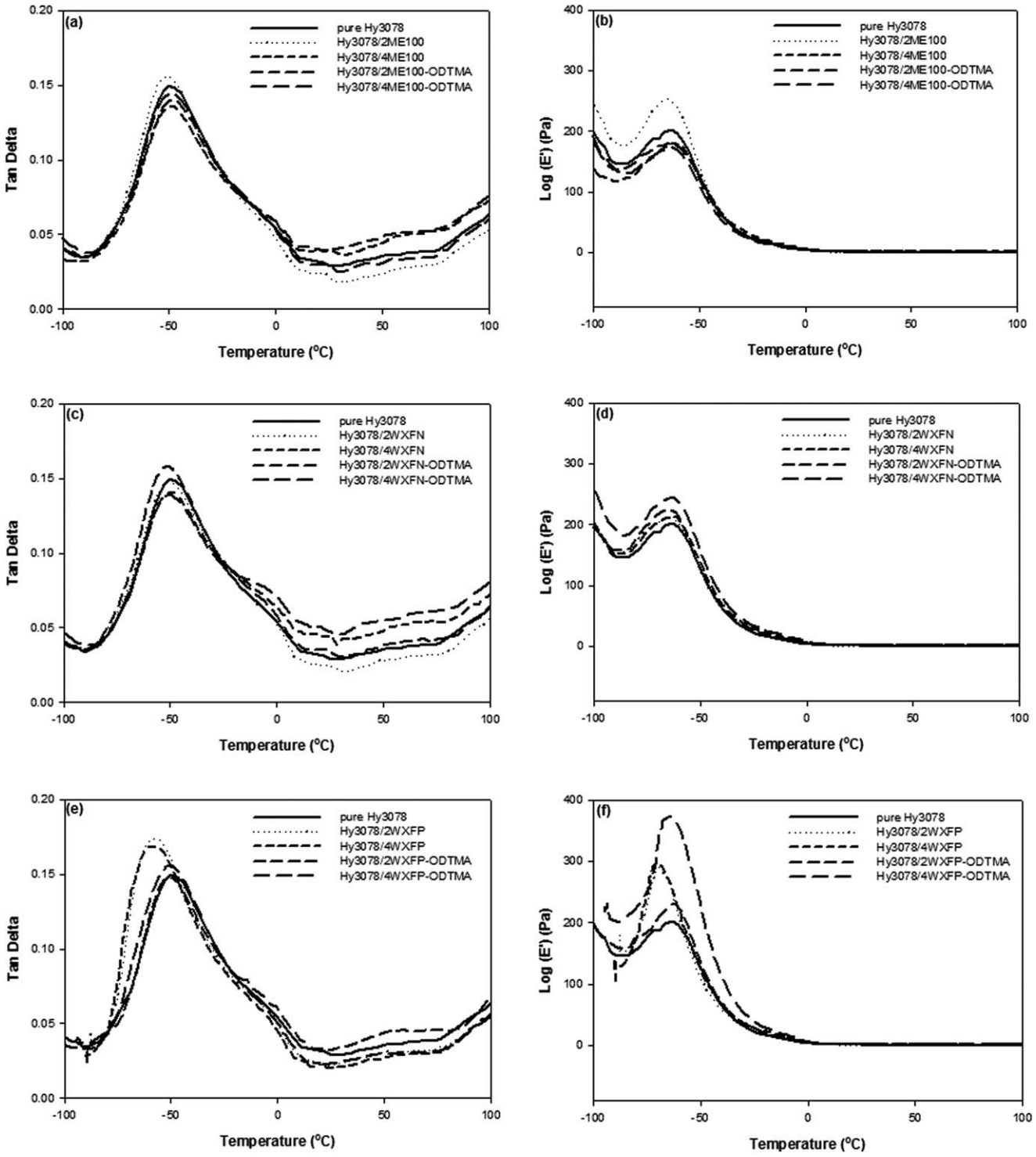

Figure 5. Tan δ and storage modulus (E′) for different Hy3078 with various clays: a, b Hy3078/ME100 and nanocomposites; c, d Hy3078/WXFN and nanocomposites; e, f Hy3078/WXFP and nanocomposites, respectively.

Hy3078 matrix. The reductions in water vapor transmission through the nanocomposites were attributed to the layered silicates providing a difficult diffusion path for the water molecules, as opposed to the layered silicates changing the diffusivity of the polymer matrix. However, improved barrier resistance has been reported with the addition of organosilicates to the polymer matrix using solution casting. Mondal *et al.*[37] incorporated cetyltrimethylammonium bromide (CTAB)-modified montmorillonite into Ecovio^{TM}, an aliphatic-aromatic copolyester that has been used in packaging film applications, and they reported large reductions in water vapor permeability. Mondal *et al.*[38,39] have also reported improved resistance to

Table VI. Water Vapor Transmission Rate at 23 °C and 100% RH

Materials	WVTR ($g/m^2.day$)
Pure Hy3078	3513.2
Hy3078/2ME100-ODTMA	1120.6
Hy3078/4ME100-ODTMA	1445.2

water vapor on addition of Na- montmorillonite nanoclay to various polymer systems, including hydroxypropylmethylcellulose, poly(vinyl alcohol) (PVA), and PVA/poly(vinyl pyrrolidone).

CONCLUSIONS

Copolyester elastomer Hytrel® 3078 was shown to be able to be melt compounded with organically modified layered silicate using twin-screw extrusion and the produce a well-dispersed nanocomposite over a series of clay loadings (1–4 wt %). The nanocomposites derived from the ME100-ODTMA high aspect ratio modified clay of 2 wt % provided the best product in terms of tensile and tear strengths and improved creep resistance. The improvement in the mechanical properties can be linked to the good dispersion and delamination achieved, in addition to the strong interaction between the TPE-E and clay. The nanoclay of the ME100-ODTMA high aspect ratio nanocomposites showed a great reduction in the water vapor transmission rate due to difficulties caused by the filler inclusions. The XRD pattern showed that Hy3078 formed an intercalated/exfoliated-type nanocomposite with all types of organoclays; except pristine clay, with which it formed a conventional composite. This is because the high compatibility between the host matrix and hydrophobic nanosilicate, which leads to good dispersion of clay in TPE-E. These dispersion profiles were confirmed with TEM observation, which showed the homogenous distribution of clay particles and aggregates in the sample cross section.

REFERENCES

1. Giannelis, E. P. *Appl. Organomet. Chem.* **1998**,*12*, 675.
2. Bhattacharya, S. N.; Kamal, M. R.; Gupta, R. K. Polymeric Nanocomposites: Theory and Practice; Hanser Gardner Pubns: Cincinnati, USA, **2008**.
3. Hytrel®, Design Guide-Module V Publication H-81098 (00.2); DuPont Engineering Polymers: Wilmington, DE.
4. Drobny, J. G. Handbook of Thermoplastic Elastomers. William Andrew Publishing: New York, USA, **2007**.
5. Walia, P.; Lawton, J.; Shogren, R.; Felker, F. *Polymer* **2000**, *41*, 8083.
6. St Lawrence, S.; Willett, J.; Carriere, C. *Polymer* **2001**, *42*, 5643.
7. Walia, P. S.; Lawton, J. W.; Shogren, R. L. *J. Appl. Polym. Sci.* **2002**, *84*, 121.
8. Versteegen, R. M.; Kleppinger, R.; Sijbesma, R. P.; Meijer, E. *Macromolecules* **2006**, *39*, 772.
9. Aso, O.; EguiazÃ¡bal, J.; Nazabal, J. *Compos. Sci. Technol.* **2007**, *67*, 2854.
10. Sreekanth, M.; Joseph, S.; Mhaske, S.; Mahanwar, P.; Bambole, V. *J. Thermoplast. Compos. Mater.* **2011**. *24*, 317.
11. Witsiepe, W. Segmented Polyester Thermoplastic Elastomers. US Patent 3,766,146, **1973**.
12. Sridhar, L. N.; Gupta, R. K.; Bhardwaj, M. *Ind. Eng. Chem. Res.* **2006**, *45*, 8282.
13. Maji, P. K.; Guchhait, P. K.; Bhowmick, A. K. *J. Mater. Sci.* **2009**, *44*, 5861.
14. Lee, C. H.; Kim, H. B.; Lim, S. T.; Choi, H. J.; Jhon, M. S. *J. Mater. Sci.* **2005**, *40*, 3981.
15. Maiti, M.; Bhattacharya, M.; Bhowmick, A. K. *Rubber Chem. Technol.* **2008**, *81*, 384.
16. Bhattacharya, M.; Bhowmick, A. K. *Polymer* **2008**, *49*, 4808.
17. LeBaron, P. C.; Wang, Z.; Pinnavaia, T. J. *Appl. Clay Sci.* **1999**, *15*, 11.
18. Sinha Ray, S.; Okamoto, K.; Okamoto, M. *Macromolecules* **2003**, *36*, 2355.
19. Yano, K.; Usuki, A.; Okada, A.; Kurauchi, T.; Kamigaito, O. *J. Polym. Sci., Part A: Polym. Chem.* **1993**, *31*, 2493.
20. Becker, O.; Cheng, Y. B.; Varley, R. J.; Simon, G. P. *Macromolecules* **2003**, *36*, 1616.
21. Kojima, Y.; Usuki, A.; Kawasumi, M.; Okada, A.; Kurauchi, T.; Kamigaito, O.; Kaji, K. J. *Polym. Sci., Part B: Polym. Phys.* **1995**, *33*, 1039.
22. Merkel, T.; Freeman, B.; Spontak, R.; He, Z.; Pinnau, I.; Meakin, P.; Hill, A. *Science* **2002**, *296*, 519.
23. Bae, J.; Lee, S.; Kim, B. C.; Cho, H. H.; Chae, D. W. *Fibers Polym.* **2013**, *14*, 729.
24. Edwards, G. A. PhD thesis, Optimisation of organically modified layered silicate based nanofillers for thermoplastic polyurethanes, The University of Queensland, **2007**.
25. Yasmin, A.; Abot, J. L.; Daniel, I. M. *Scr. Mater.* **2003**, *49*, 81.
26. Breu, J.; Seidl, W.; Stoll, A. J.; Lange, K. G.; Probst, T. U. *Chem. Mater.* **2001**, *13*, 4213.
27. Yang, J. H.; Han, Y. S.; Choy, J. H.; Tateyama, H. *J. Mater. Chem.* **2001**, *11*, 1305.
28. Osman, A. F.; Edwards, G. A.; Schiller, T. L.; Andriani, Y.; Jack, K. S.; Morrow, I. C.; Halley, P. J.; Martin, D. J. *Macromolecules* **2011**, *45*, 198.
29. Liu, L.; Jia, D.; Luo, Y.; Guo, B. *J. Appl. Polym. Sci.* **2006**, *100*, 1905.
30. Shen, Z.; Simon, G. P.; Cheng, Y. B. *Polymer* **2002**, *43*, 4251.
31. Százdi, L.; Pozsgay, A.; Pukánszky, B. *Eur. Polym. J.* **2007**, *43*, 345.
32. Chung, S. C.; Hahm, W. G.; Im, S. S.; Oh, S. G. *Macromol. Res.* **2002**, *10*, 221.
33. Reddy, C.; Das, C.; Narkis, M. *Polym. Compos.* **2005**, *26*, 806.
34. Wegner, G.; Fujii, T.; Meyer, W.; Lieser, G. *Die Angew. Makromol. Chem.* **1978**, *74*, 295.

35. Arrighi, V.; McEwen, I.; Qian, H.; Serrano Prieto, M. *Polymer* **2003**, *44*, 6259.

36. Szymczyk, A. *J. Appl. Polym. Sci.* **2012**, *126*, 796.

37. Mondal, D.; Bhowmick, B.; Mollick, M. M. R.; Maity, D.; Saha, N. R.; Rangarajan, V.; Rana, D.; Sen, R.; Chattopadhyay, D. *J. Appl. Polym. Sci.* **2014**, *131*, 40079.

38. Mondal, D.; Bhowmick, B.; Mollick, Md. M. R.; Maity, D.; Mukhopadhyay, A.; Rana, D.; Chattopadhyay, D. *Carbohydr. Polym.* **2013**, *96*, 57.

39. Mondal, D.; Mollick, M. M. R.; Bhowmick, B.; Maity, D.; Bain, M. K.; Rana, D.; Mukhopadhyay, A.; Dana, K.; Chattopadhyay, D. *Prog. Nat. Sci. Mater. Int.* **2013**, *23*, 579.